



Towards the design of monolithic decoupled XYZ compliant parallel mechanisms for multi-function applications

G. Hao

Department of Electrical and Electronic Engineering, School of Engineering,
University College Cork, Cork, Ireland

Correspondence to: G. Hao (g.hao@ucc.ie)

Received: 30 January 2013 – Accepted: 19 April 2013 – Published: 15 August 2013

Abstract. This paper deals with the monolithic decoupled XYZ compliant parallel mechanisms (CPMs) for multi-function applications, which can be fabricated monolithically without assembly and has the capability of kinetostatic decoupling. At first, the conceptual design of monolithic decoupled XYZ CPMs is presented using identical spatial compliant multi-beam modules based on a decoupled 3-PPPR parallel kinematic mechanism. Three types of applications: motion/positioning stages, force/acceleration sensors and energy harvesting devices are described in principle. The kinetostatic and dynamic modelling is then conducted to capture the displacements of any stage under loads acting at any stage and the natural frequency with the comparisons with FEA results. Finally, performance characteristics analysis for motion stage applications is detailed investigated to show how the change of the geometrical parameters can affect the performance characteristics, which provides initial optimal estimations. Results show that the smaller thickness of beams and larger dimension of cubic stages can improve the performance characteristics excluding natural frequency under allowable conditions. In order to improve the natural frequency characteristic, a monolithic decoupled configuration that is achieved through employing more beams in the spatial modules or reducing the mass of each cubic stage mass can be adopted. In addition, an isotropic variation with different motion range along each axis and same payload in each leg is proposed. The redundant design for monolithic fabrication is introduced in this paper, which can overcome the drawback of monolithic fabrication that the failed compliant beam is difficult to replace, and extend the CPM's life.

1 Introduction

Compliant parallel mechanisms (CPMs) transmit motion/loads by deformation of their compliant links (namely jointless), and belong to a class of parallel-type mechanisms. They aim to utilize the material compliance/flexibility instead of only analyzing/suppressing the negative flexibility effect like those initial works in the area of kinematics of mechanisms with elasticity (Howell, 2001; Hao, 2011). This revolutionary change leads to many potential merits such as reduced part count (monolithic), zero backlashes, no need for lubrication, reduced wear, high precision and compact configuration in comparison with the rigid-body counterparts. CPMs with multiple DoF (degrees of freedom) have drawn

more attentions from academia and industries due to their extensive applications such as motion/positioning stages (Awtar and Slocum, 2007; Dong et al., 2007; Hao and Kong, 2012a, b), acceleration/force sensors (Gao and Zhang, 2010; Hansen et al., 2007; Cappelleri et al., 2010) and energy harvesting devices (Rupp et al., 2009; Ando et al., 2010).

For a planar multi-DoF CPM such as the XY CPM, it is always easy to fabricate towards a monolithic configuration using existing well-developed planar manufacturing technologies such as wire EDM, water jet, and laser cutting (Awtar, 2004). However, these manufacturing technologies usually fail to satisfy the needs of fabricating most spatial multi-DoF CPMs (such as XYZ CPMs) monolithically, and therefore assembly has to be passively applied as shown in (Dong et

al., 2007; Hao and Kong, 2012b; Gao and Zhang, 2010), which leads to some issues such as assembly error, increased number of parts, reduced stiffness (by about 30% by bolted joints), and increased cost (Hao and Kong, 2012b). Over recent years, 3-D printing technology has been developed rapidly. Various base/substrate materials, such as engineering plastics, ceramics and metal, can be used for fabrication for a variety of applications. But the emerging 3-D printing technology may lead to limited or undesired performance characteristics of material due to no traditional heat treatment applied and inherent layer-by-layer fabrication. This shortcoming has been proved by testing our initial prototype, made of engineering plastic, obtained using a 3-D printer. Therefore, better manufacturing approaches/strategies for spatial multi-DoF CPMs are potentially needed. Averting the manufacturing issue on spatial CPMs, one can design a type of spatial multi-DoF CPMs that are possible to be fabricated monolithically using the above planar manufacturing technologies without bringing any assembly issues.

In this paper, we will mainly deal with the XYZ CPMs with (kinetostatically) decoupled configuration. Kinetostatic decoupling means that one primary output translational displacement is only affected by the actuation force along the same direction, which describes the relationship between the input force and output motion. This decoupling (not absolute) is also called the output-decoupling/minimal cross-axis coupling in CPMs. Kinetostatic coupling may lead to complicated motion control, which is the sufficient condition of kinematic decoupling. A number of literatures have reported the design of decoupled XYZ CPMs for motion/positioning stage and sensing applications (Hao and Kong, 2009, 2012b; Gao and Zhang, 2010; Li and Xu, 2011; Pham et al., 2006; Yue et al., 2010; Tang et al., 2006) using kinematics design methods (Hao, 2011). Here, each of the three kinematic legs/chains, which are coupled in parallel, is individually a serial-parallel hybrid arrangement. But none of them have showed the possibility for monolithic fabrication. Also, these designs have their own limitations such small motion range (Li and Xu, 2011; Pham et al., 2006; Yue et al., 2010), bulky and complex configuration (due to the serial-parallel hybrid arrangement) (Li and Xu, 2011; Pham et al., 2006; Hao and Kong, 2009; Tang et al., 2006), and poor out-of-plane stiffness of the PP plane in each leg (Li and Xu, 2011; Pham et al., 2006; Hao and Kong, 2009; Yue et al., 2010; Tang et al., 2006). Recently, Awtar et al. (2013) proposed a novel XYZ parallel kinematic flexure mechanism with geometrically decoupled DoF using identical flexure plates, which has a more compact and simpler construction and has the possibility to be fabricated monolithically. However, this design suffers from complicated modelling, bad out-of-plane stiffness and big lost motion, especially its three actuation directions are skew and cannot intersect at the center of the primary motion stage so that its applications are limited in low payload, and/or low speed. Hao and Kong (2012b) re-

ported a decoupled XYZ CPM composed of identical spatial modules, but still has the challenging issue on fabrication.

This work builds on the above advances on decoupled XYZ CPMs towards a monolithic configuration (also compact and simple) for manufacturing purpose. It also stresses the potential extensive applications in multi-axis motion/positioning stages, multi-axis sensors (acceleration/force), and energy harvesting devices using the present monolithic decoupled XYZ CPMs.

This paper is organized as follows. Section 2 proposes the conceptual design of monolithic decoupled XYZ CPMs for three-type applications: motion/positioning stages, acceleration/force sensors, and energy harvesting devices at first. Then the analytical kinetostatic and dynamic modelling is undertaken in Sect. 3. In Sect. 4, the performance characteristics analysis to reflect the change of performance characteristics with that of the geometrical parameters is investigated. Section 5 discusses the thermal stability. Conclusions are drawn in Sect. 6.

2 Conceptual design of monolithic decoupled XYZ CPMs for multi-function applications

2.1 Monolithic decoupled XYZ CPMs

A decoupled XYZ CPM for the motion/positioning stage can be generated using a design approach proposed in the references (Hao, 2011; Hao and Kong, 2012b). This design is demonstrated in Fig. 1, which is based on a decoupled XYZ parallel kinematic mechanism (PKM) whose three planes associated with the passive PPR kinematic chains are orthogonal. It is obtained by replacing the actuated P joint and the passive PPR chain in each leg of the 3-PPPR XYZ PKM (Fig. 1a) with the compliant P joint in Fig. 1c and a compliant PPR joint in Fig. 1b, respectively, and making appropriate arrangement for the identical building blocks (spatial four-beam modules).

In order to facilitate the monolithic fabrication, an improved design of the decoupled XYZ CPMs (Fig. 2) is adopted in terms of the proposed decoupled XYZ CPM (Fig. 1d), which can be fabricated monolithically from a cubic material by three orthogonal directions' cutting using EDM/milling machining for a macro-version, or lithography/DRIE for an MEMS version with same masks on three surfaces of the cube. The improved design is composed of eight rigid cubic stages organically connected by twelve identical spatial multi-beam modules with planar motion to form a monolithic and compact cubic configuration. When four adjacent rigid stages are fixed in the undeformed configuration (and therefore three spatial modules are inactive), the other four rigid stages act as the mobiles stages (X-, Y-, Z-, and XYZ-stages), displaced by the deformation of the nine spatial modules, to achieve the function of XYZ CPMs.

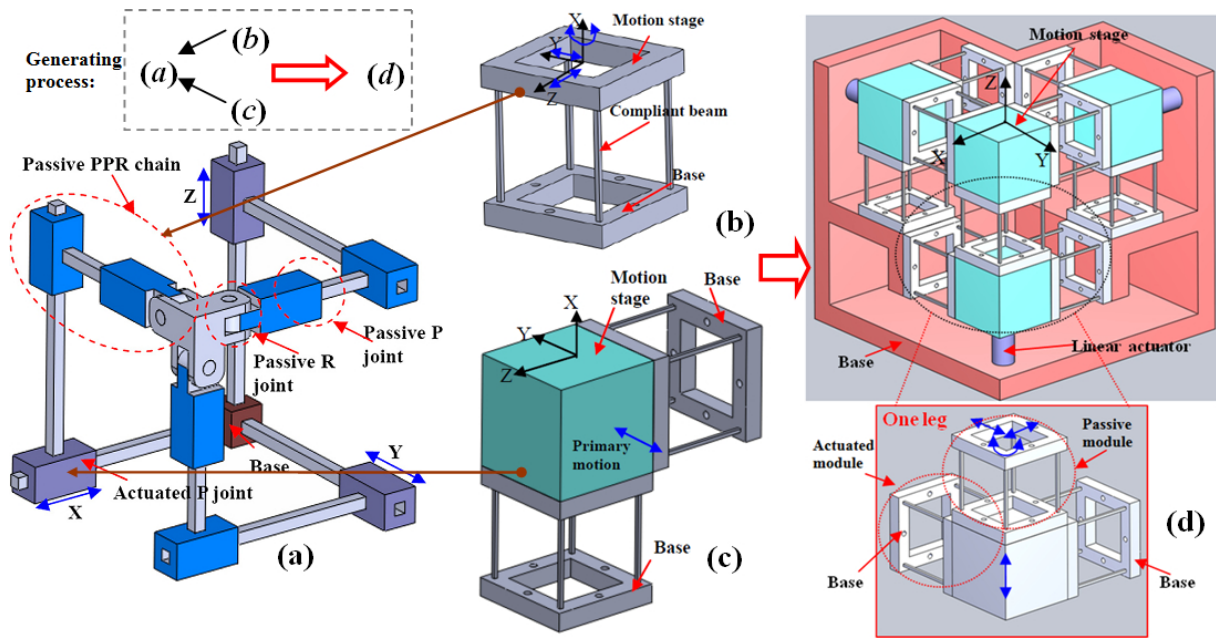


Figure 1. The generating process of a decoupled XYZ CPM: (a) A decoupled 3-PPPR XYZ PKM (Hao, 2011; Hao and Kong, 2012b) with three planes associated with the passive PPR kinematic chains orthogonal; (b) A compliant planar-motion PPR joint (Hao, 2011; Hao et al., 2011; Hao and Kong, 2013): spatial four-beam module that is composed four identical symmetrical square wire beams spaced around a circle uniformly; (c) A compliant P joint (Hao, 2011; Hao and Kong, 2012b): two spatial four-beam modules connected in parallel, two planes associated two PPR joints of which are orthogonal; (d) A decoupled XYZ CPM using identical spatial four-beam modules.

Three different monolithic forms are shown in Fig. 2a, b and c, respectively. As mentioned earlier, the monolithic decoupled XYZ CPM (for instance, Fig. 2a) has mainly three types of applications: motion/positioning stages, acceleration/force sensors, and energy harvesting devices, which is detailed as follows.

2.1.1 High-precision motion/positioning stages

For the applications as high-precision motion/positioning stages, the proposed monolithic decoupled XYZ CPM (Fig. 2a) can be actuated by three linear Voice Coil (VC) actuators for large motion range or by three PZT actuators for small motion range as shown in Fig. 1d. In addition three optical linear encoders (input sensing) and three capacitive measuring systems (output sensing) are required.

2.1.2 Acceleration/force sensors

The presented monolithic decoupled XYZ CPM (Fig. 2a) can be used as the 3-axis acceleration/force sensor without using linear actuators. For the use as the force sensor, any external force exerted at the XYZ-stage along each axis can be sensed by measuring the displacements of the X-, Y- and Z- stages along the X-, Y-, and Z-axes, respectively, by piezoresistors or other types of sensors. When used as the acceleration sensor, the XYZ-, X-, Y- and Z-stages are served as the inertial mass of the sensor. If there is an acceleration along certain

resultant direction, the components of the resultant inertial force along the X-, Y-, and Z-axes will result from the contribution of the combined mass of the XYZ- and X-stages, that of the XYZ- and Y-stages, and that of the of the XYZ- and Z-stages, respectively. Then by sensing displacements of the X-, Y- and Z-stages along the X-, Y-, and Z-axes, respectively, one can obtain the inertial force along each axis and then work out the acceleration along each axis.

2.1.3 Energy harvesting devices

Coupling with magnets and coils, an example 3-axis energy harvesting device (Fig. 3) can be obtained based on the monolithic decoupled XYZ CPM (Fig. 2a). It harvests energy in three axes through the well-known electromagnetic induction. If there is an external excitation along a certain axis, the inertial mass (including the magnet) coupled with the compliant members (spring) along this axis will produce a vibration to make the magnet to go through the coil, and then magnetic flux changes with time, which induces the electricity production for harvesting.

2.2 Redundant design for monolithic fabrication

A major drawback of the monolithic fabrication is that the failure (yield/fraction) of certain compliant beam(s) can cause the whole system's permanent strike due to the fact that the failed wire beam is difficult to replace. However, the

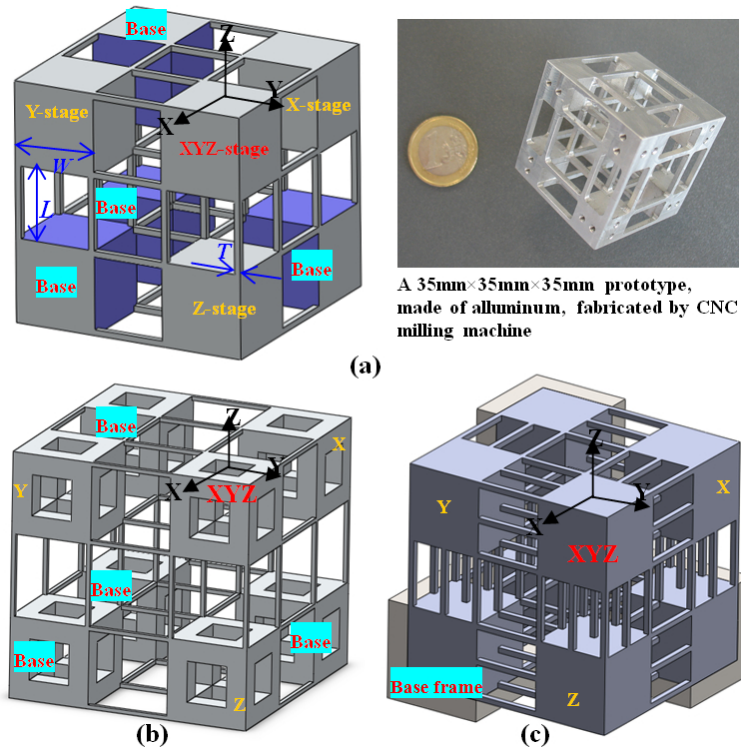


Figure 2. Monolithic decoupled XYZ CPMs: (a) a monolithic decoupled XYZ CPM with three geometrical parameters; (b) a monolithic decoupled XYZ CPM with improved natural frequency via reducing the cubic stage mass; and (c) a monolithic decoupled XYZ CPM with improved natural frequency via increasing the beam number (i.e. stiffness enhanced) (all configurations have same motion range).

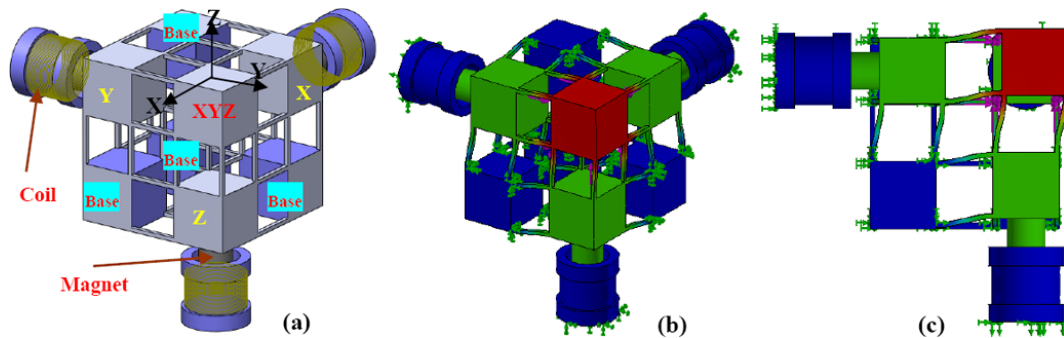


Figure 3. Energy harvesting devices: (a) Energy harvesting device based on a monolithic decoupled XYZ CPM; (b) Perspective view of FEA results in deformation; (c) Top view of FEA results in deformation.

present monolithic decoupled XYZ CPM in this paper is a redundant design with three redundant spatial four-beam modules inactive (or four cubic stages fixed), and therefore the redundant building blocks (or fixed cubic stages) can swap the functions with certain failure’s mobile building blocks (or mobile cubic stages) to extend the system life.

In our design, each of three passive spatial four-beam modules undergoes two translations, and is prone to fail compared to other spatial modules to produce only one translation. If either of the three passive spatial four-beam modules fails, the base frame originally connecting the four fixed cu-

bic stages can be moved to connect with the four originally mobile cubic stages in their initially undeformed configuration. Such a way, the life of the XYZ CPM is retrieved. A more clear illustration is shown in Fig. 4.

2.3 Variation for the monolithic decoupled XYZ CPM

It is easy to understand that the above proposed monolithic decoupled XYZ CPM have same motion range along each axis, i.e. a cubic workspace. However, for the purposes that the motion range in a certain direction is required larger/smaller than the other(s) and also that each leg has

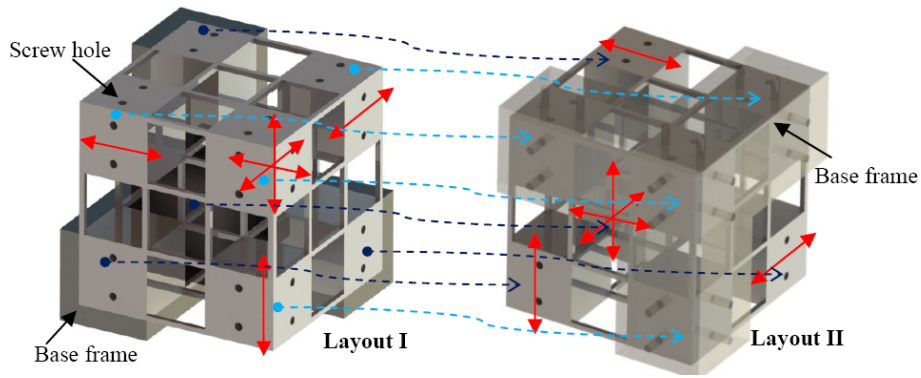


Figure 4. Demonstration of redundant design (rendered).

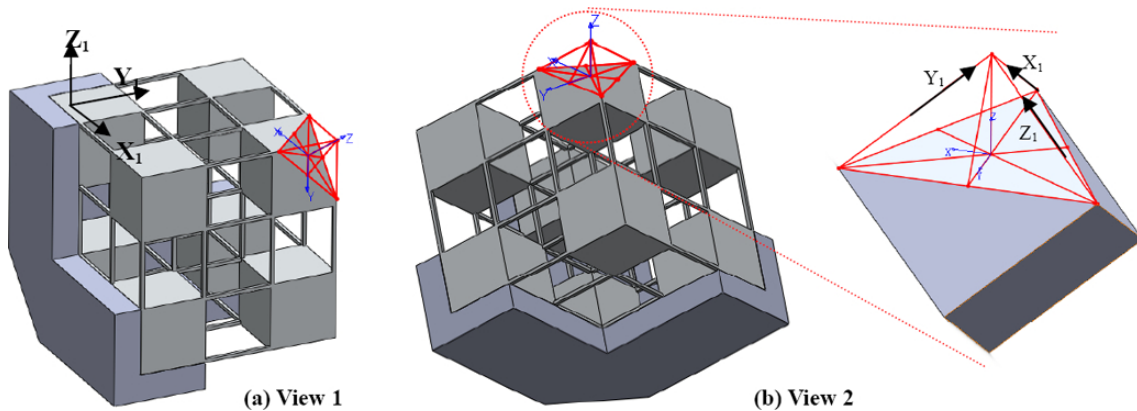


Figure 5. A variation for the monolithic decoupled XYZ CPM.

same payload (isotropic) (Kong and Gosselin, 2002; Werner et al., 2010), a variation can be made from the present monolithic decoupled XYZ CPM as shown in Fig. 5.

This variation has the decoupling property with regard to the original coordinate system $X_1 Y_1 Z_1$. But in the new coordinate system XYZ , the motion is not decoupled. The motion relationships between the two coordinate systems will be followed in the subsequent section.

3 Modelling of the monolithic decoupled XYZ CPM

In order to analyzing the performance characteristics of the monolithic decoupled XYZ CPM (Fig. 2a), it is essential to carry out the kinetostatic modelling and dynamic modelling.

3.1 Kinetostatic modelling

References (Hao, 2011; Hao and Kong, 2012b) have given the detailed analytical modelling derivation for an XYZ CPM using identical spatial double four-beam modules, therefore, in this paper, we will directly use the associated linear equations from these references with different geometrical parameters substitution. The purpose for linear kinetostatic

modelling is to approximately estimate the displacements of the centers of the XYZ-, X-, Y-, and Z-stages under the action of loads at the centers of those stages to suit different applications. Here, the normalization-based strategy (Hao et al., 2011; Hao and Kong, 2013) is also adopted to represent loads and displacements using the corresponding lower-case letters, which refers to that all translational displacements and length parameters are normalized by the beam actual length L , forces by EI/L^2 , and moments by EI/L . Here, E and I denotes the Young's modulus and the second moment of the area of a symmetrical cross-section, respectively.

The compliance matrix for the CPM system (Fig. 2a) with regard to the center of the XYZ-stage in the global coordinate system XYZ , i.e. the loads and displacements are both defined at the center, is obtained as

$$\mathbf{C}_{\text{cpm}} = \mathbf{K}_{\text{cpm}}^{-1} = (\mathbf{R}_{\text{leg1}} \mathbf{K}_{\text{leg2}} \mathbf{R}_{\text{leg1}}^{-1} + \mathbf{K}_{\text{leg2}} + \mathbf{R}_{\text{leg3}} \mathbf{K}_{\text{leg2}} \mathbf{R}_{\text{leg3}}^{-1})^{-1} \quad (1)$$

where \mathbf{C}_{cpm} and \mathbf{K}_{cpm} are the compliance and stiffness matrices of the CPM system, respectively; \mathbf{K}_{leg2} is the stiffness matrix of Leg 2 (with the Y-stage) defined at the center of XYZ-stage in the global coordinate system, which is also a reference based on which the stiffness (or compliance) matrices for Legs 1 and 3 can be obtained by appropriate coordinate

transformation so that $\mathbf{K}_{leg1} = \mathbf{R}_{leg1} \mathbf{K}_{leg2} \mathbf{R}_{leg1}^{-1}$, and $\mathbf{K}_{leg3} = \mathbf{R}_{leg3} \mathbf{K}_{leg2} \mathbf{R}_{leg3}^{-1}$; \mathbf{R}_{leg1} and \mathbf{R}_{leg3} are the rotation transformation matrices for Legs 1 and 3, respectively, which are given as

$$\mathbf{R}_{leg1} = \begin{bmatrix} \mathbf{R}_Z(-\pi/2)_{3 \times 3} & \mathbf{0}_{3 \times 3} \\ \mathbf{0}_{3 \times 3} & \mathbf{R}_Z(-\pi/2)_{3 \times 3} \end{bmatrix} \times \begin{bmatrix} \mathbf{R}_Y(-\pi/2)_{3 \times 3} & \mathbf{0}_{3 \times 3} \\ \mathbf{0}_{3 \times 3} & \mathbf{R}_Y(-\pi/2)_{3 \times 3} \end{bmatrix},$$

and

$$\mathbf{R}_{leg3} = \begin{bmatrix} \mathbf{R}_Y(\pi/2)_{3 \times 3} & \mathbf{0}_{3 \times 3} \\ \mathbf{0}_{3 \times 3} & \mathbf{R}_Y(\pi/2)_{3 \times 3} \end{bmatrix} \times \begin{bmatrix} \mathbf{R}_Z(\pi/2)_{3 \times 3} & \mathbf{0}_{3 \times 3} \\ \mathbf{0}_{3 \times 3} & \mathbf{R}_Z(\pi/2)_{3 \times 3} \end{bmatrix}.$$

The stiffness matrix of Leg 2 can be represented as

$$\mathbf{K}_{leg2} = [\mathbf{J}_{m3}(\mathbf{R}_{pp} \mathbf{C}_m \mathbf{R}_{pp}^{-1}) \mathbf{J}_{m3}^T + \mathbf{J}_p \mathbf{C}_p \mathbf{J}_p^T]^{-1} \quad (2)$$

where \mathbf{C}_m is the compliance matrix of the spatial four-beam module (compliant PPR joint, Fig. 1b) in Leg 2 with regard to the center of the bottom-plane of its own motion stage in its own local coordinate system; \mathbf{C}_p is the compliance matrix of the compliant P joint (Fig. 1c) in Leg 2 with regard to the Y-stage center in the global coordinate system; \mathbf{J}_{m3} and \mathbf{J}_p are the position transformation matrices, and \mathbf{R}_{pp} is the rotation transformation matrix, which are detailed below:

$$\mathbf{J}_{m3} = \begin{bmatrix} \mathbf{I}_{3 \times 3} & \begin{bmatrix} 0 & 0 & -w/2 \\ 0 & 0 & 0 \\ w/2 & 0 & 0 \end{bmatrix} \\ \mathbf{0}_{3 \times 3} & \mathbf{I}_{3 \times 3} \end{bmatrix},$$

$$\mathbf{J}_p = \begin{bmatrix} \mathbf{I}_{3 \times 3} & \begin{bmatrix} 0 & 0 & -1-w \\ 0 & 0 & 0 \\ 1+w & 0 & 0 \end{bmatrix} \\ \mathbf{0}_{3 \times 3} & \mathbf{I}_{3 \times 3} \end{bmatrix}, \quad \text{and}$$

$$\mathbf{R}_{pp} = \begin{bmatrix} \mathbf{R}_Z(\pi/2)_{3 \times 3} & \mathbf{0}_{3 \times 3} \\ \mathbf{0}_{3 \times 3} & \mathbf{R}_Z(\pi/2)_{3 \times 3} \end{bmatrix}.$$

The compliance matrix of the compliant P joint is further represented as

$$\mathbf{C}_p = \{(\mathbf{J}_{m1} \mathbf{C}_m \mathbf{J}_{m1}^T)^{-1} + [\mathbf{J}_{m2}(\mathbf{R}_m \mathbf{C}_m \mathbf{R}_m^{-1}) \mathbf{J}_{m2}^T]^{-1}\}^{-1} \quad (3)$$

where \mathbf{J}_{m1} and \mathbf{J}_{m2} are the position transformation matrices, and \mathbf{R}_m is the rotation transformation matrix, which are ex-

pressed below:

$$\mathbf{J}_{m1} = \begin{bmatrix} \mathbf{I}_{3 \times 3} & \begin{bmatrix} 0 & 0 & 0 \\ 0 & 0 & w/2 \\ 0 & -w/2 & 0 \end{bmatrix} \\ \mathbf{0}_{3 \times 3} & \mathbf{I}_{3 \times 3} \end{bmatrix},$$

$$\mathbf{J}_{m2} = \begin{bmatrix} \mathbf{I}_{3 \times 3} & \begin{bmatrix} 0 & w/2 & 0 \\ -w/2 & 0 & 0 \\ 0 & 0 & 0 \end{bmatrix} \\ \mathbf{0}_{3 \times 3} & \mathbf{I}_{3 \times 3} \end{bmatrix}, \quad \text{and}$$

$$\mathbf{R}_m = \begin{bmatrix} \mathbf{R}_Y(\pi/2)_{3 \times 3} & \mathbf{0}_{3 \times 3} \\ \mathbf{0}_{3 \times 3} & \mathbf{R}_Y(\pi/2)_{3 \times 3} \end{bmatrix} \times \begin{bmatrix} \mathbf{R}_Z(\pi)_{3 \times 3} & \mathbf{0}_{3 \times 3} \\ \mathbf{0}_{3 \times 3} & \mathbf{R}_Z(\pi)_{3 \times 3} \end{bmatrix}.$$

The compliance matrix of the spatial four-beam module is further derived as

$$\mathbf{C}_m = \left(\sum_{i=0}^4 \mathbf{D}_i^T \mathbf{K} \mathbf{D}_i \right)^{-1} \quad (4)$$

where

$$\mathbf{D}_i = \begin{bmatrix} \mathbf{I}_{3 \times 3} & \begin{bmatrix} 0 & z'_i & -y'_i \\ -z'_i & 0 & x'_i \\ y'_i & -x'_i & 0 \end{bmatrix} \\ \mathbf{0}_{3 \times 3} & \mathbf{I}_{3 \times 3} \end{bmatrix}, \quad \text{and}$$

$$\mathbf{K} = \begin{bmatrix} d & 0 & 0 & 0 & 0 & 0 \\ 0 & 12 & 0 & 0 & 0 & -6 \\ 0 & 0 & 12 & 0 & 6 & 0 \\ 0 & 0 & 0 & 1/(1+\nu) & 0 & 0 \\ 0 & 0 & 6 & 0 & 4 & 0 \\ 0 & -6 & 0 & 0 & 0 & 4 \end{bmatrix}.$$

Here, $x'_1 = 0$, $y'_1 = (w-t)/2$, and $z'_1 = (w-t)/2$; $x'_2 = 0$, $y'_2 = (w-t)/2$, and $z'_2 = -(w-t)/2$; $x'_3 = 0$, $y'_3 = -(w-t)/2$, and $z'_3 = -(w-t)/2$; $x'_4 = 0$, $y'_4 = -(w-t)/2$, and $z'_4 = (w-t)/2$. $d = 12/(t)^2$ for square cross-section with normalized thickness t . ν is the Poisson's ratio of the material.

Based on the above modelling results, the relationships between the displacements at the center of the XYZ-stage and the loads acting at both the actuation points and the centers of the XYZ-, X-, Y-, and Z-stages are derived as

$$\mathbf{F} = \mathbf{K}_{cpm} \mathbf{X}_s - \mathbf{K}_{leg1} \mathbf{R}_{leg1} (\mathbf{J}_p \mathbf{C}_p \mathbf{J}_p^T) \mathbf{R}_{leg1}^{-1} \mathbf{J}_{pa1}^T \mathbf{F}_{ax} - \mathbf{K}_{leg2} (\mathbf{J}_p \mathbf{C}_p \mathbf{J}_p^T) \mathbf{J}_{pa2}^T \mathbf{F}_{ay} - \mathbf{K}_{leg3} \mathbf{R}_{leg3} (\mathbf{J}_p \mathbf{C}_p \mathbf{J}_p^T) \mathbf{R}_{leg3}^{-1} \mathbf{J}_{pa3}^T \mathbf{F}_{az},$$

i.e.

$$\mathbf{X}_s = \mathbf{C}_{cpm} \left[\mathbf{F} + \mathbf{K}_{leg1} \mathbf{R}_{leg1} (\mathbf{J}_p \mathbf{C}_p \mathbf{J}_p^T) \mathbf{R}_{leg1}^{-1} \mathbf{J}_{pa1}^T \mathbf{F}_{ax} + \mathbf{K}_{leg2} \times (\mathbf{J}_p \mathbf{C}_p \mathbf{J}_p^T) \mathbf{J}_{pa2}^T \mathbf{F}_{ay} + \mathbf{K}_{leg3} \mathbf{R}_{leg3} (\mathbf{J}_p \mathbf{C}_p \mathbf{J}_p^T) \mathbf{R}_{leg3}^{-1} \mathbf{J}_{pa3}^T \mathbf{F}_{az} \right] \quad (5)$$

where $\mathbf{F} = [f_x, f_y, f_z, m_x, m_y, m_z]^T$ and $\mathbf{X}_s = [x_s, y_s, z_s, \theta_{sx}, \theta_{sy}, \theta_{sz}]^T$ which are the load-vector and displacement-vector are first defined at the center of the XYZ-stage;

$\mathbf{F}_{ax} = [f_{ax-x}, f_{ax-y}, f_{ax-z}, m_{ax-x}, m_{ax-y}, m_{ax-z}]^T$,
 $\mathbf{F}_{ay} = [f_{ay-x}, f_{ay-y}, f_{ay-z}, m_{ay-x}, m_{ay-y}, m_{ay-z}]^T$, and
 $\mathbf{F}_{az} = [f_{az-x}, f_{az-y}, f_{az-z}, m_{az-x}, m_{az-y}, m_{az-z}]^T$, which denote the load vectors at the centers of the X-, Y- and Z-stages, respectively. As an example for explaining the force symbols, f_{ax-x} , f_{ax-y} and f_{ax-z} denote the forces acting at the center of the X-stage along the X-, Y-, and Z-axes, respectively;

\mathbf{J}_{pai} ($i = 1, 2, 3$) in Eq. (5) is the position transformation matrix for loads in each leg, which is shown below

$$\mathbf{J}_{pai} = \begin{bmatrix} \mathbf{I}_{3 \times 3} & \begin{bmatrix} 0 & z'_i & -y'_i \\ -z'_i & 0 & x'_i \\ y'_i & -x'_i & 0 \end{bmatrix} \\ \mathbf{0}_{3 \times 3} & \mathbf{I}_{3 \times 3} \end{bmatrix}.$$

Where, $x'_1 = -(1+w)$, $y'_1 = 0$, and $z'_1 = 0$; $x'_2 = 0$, $y'_2 = -(1+w)$, and $z'_2 = 0$; $x'_3 = 0$, $y'_3 = 0$, and $z'_3 = -(1+w)$.

We can then obtain the displacements at the centers of the X-, Y-, and Z-stages as

$$\begin{aligned} \mathbf{X}_{ax} &= \mathbf{R}_{leg1} \mathbf{C}_p \mathbf{R}_{leg1}^{-1} \mathbf{J}_{p1}^T [\mathbf{K}_{leg1} (\mathbf{X}_s - \mathbf{R}_{leg1} (\mathbf{J}_p \mathbf{C}_p \mathbf{J}_p^T) \\ &\quad \times \mathbf{R}_{leg1}^{-1} \mathbf{J}_{pa1}^T \mathbf{F}_{ax}) + \mathbf{J}_{pa1}^T \mathbf{F}_{ax}], \\ \mathbf{X}_{ay} &= \mathbf{C}_p \mathbf{J}_{p2}^T [\mathbf{K}_{leg2} (\mathbf{X}_s - \mathbf{J}_p \mathbf{C}_p \mathbf{J}_p^T \mathbf{J}_{pa2}^T \mathbf{F}_{ay}) + \mathbf{J}_{pa2}^T \mathbf{F}_{ay}], \\ \mathbf{X}_{az} &= \mathbf{R}_{leg3} \mathbf{C}_p \mathbf{R}_{leg3}^{-1} [\mathbf{K}_{leg3} (\mathbf{X}_s - \mathbf{R}_{leg3} \\ &\quad \times (\mathbf{J}_p \mathbf{C}_p \mathbf{J}_p^T) \mathbf{R}_{leg3}^{-1} \mathbf{J}_{pa3}^T \mathbf{F}_{az}) + \mathbf{J}_{pa3}^T \mathbf{F}_{az}] \end{aligned} \quad (6)$$

where $\mathbf{X}_{ax} = [x_{ax}, y_{ax}, z_{ax}, \theta_{ax-x}, \theta_{ax-y}, \theta_{ax-z}]^T$,

$\mathbf{X}_{ay} = [x_{ay}, y_{ay}, z_{ay}, \theta_{ay-x}, \theta_{ay-y}, \theta_{ay-z}]^T$, and

$\mathbf{X}_{az} = [x_{az}, y_{az}, z_{az}, \theta_{az-x}, \theta_{az-y}, \theta_{az-z}]^T$, which denote the displacement vectors at the centers of the X-, Y- and Z-stages. As an example for explaining the displacement symbols, x_{ay} , y_{ay} , and z_{ay} denote the translational displacements of the Y-stage center along the X-, Y- and Z-axes, respectively; \mathbf{J}_{pi} ($i = 1, 2, 3$) is the position transformation matrix for loads in each leg as

$$\mathbf{J}_{pi} = \begin{bmatrix} \mathbf{I}_{3 \times 3} & \begin{bmatrix} 0 & z'_i & -y'_i \\ -z'_i & 0 & x'_i \\ y'_i & -x'_i & 0 \end{bmatrix} \\ \mathbf{0}_{3 \times 3} & \mathbf{I}_{3 \times 3} \end{bmatrix}.$$

Here, $x'_1 = (1+w)$, $y'_1 = 0$, and $z'_1 = 0$; $x'_2 = 0$, $y'_2 = (1+w)$, and $z'_2 = 0$; $x'_3 = 0$, $y'_3 = 0$, and $z'_3 = (1+w)$.

It should be noted that the above derived analytical models are capable of comprehensively reflecting the displacements of any stage under loading at any stage, and are accurate enough under small motion range. The proposed analytical models can be used for quick design synthesis, and also offer a reference for further nonlinear kinetostatic analysis and optimization.

3.2 Dynamic modelling

Accurate dynamic equations can be obtained from the classical Lagrange equation building on the above kinetostatic modelling results. However, we only give approximate estimations of the natural frequencies of the monolithic decoupled XYZ CPM using simplified stiffness models.

The actual primary translational stiffness along each axis can be simplified as

$$K = 16 \frac{12EI}{L^3} = 16 \frac{ET^4}{L^3}. \quad (7)$$

Then the equal first, second or third-order natural frequency is derived as

$$f_1 = \sqrt{K/(M)}/(2\pi) \quad (8)$$

where M is the actual motion mass along each axis only considering two stages neglecting the compliant beams' mass.

Given that all stages are identical, M is double of mass of each (cubic) stage, which is equal to $2\rho W^3$ with a density of ρ . So Eq. (8) is rewritten as

$$f_1 = \sqrt{8ET^4/(\rho W^3 L^3)}/(2\pi) = \sqrt{8Et^4/(\rho w^3 L^2)}/(2\pi). \quad (9)$$

3.3 Results analysis

Let the material be a standard aluminum alloy AL 6061-T651 with Young's Modules $E = 69$ Gpa and Poisson's ratio $\nu = 0.33$. Also, we define the geometrical parameters as: $L = 20$ mm (beam length), $W = 20$ mm (cubic stage's side-length), $T = 1$ mm (beam thickness) (i.e. a system dimension of 60 mm \times 60 mm \times 60 mm) for the initial performance analysis.

Given an example of only three forces acting at the centers of the X-, Y- and Z-stages for the motion stage applications, the normalized load-displacement relationships based on Eqs. (5) and (6) can be expressed as

$$\begin{bmatrix} x_s \\ y_s \\ z_s \\ \theta_{sx} \\ \theta_{sy} \\ \theta_{sz} \end{bmatrix} = \mathbf{C}_{a-s} \begin{bmatrix} f_{ax-x} \\ f_{ay-y} \\ f_{az-z} \\ f_{ax-x} \\ f_{ay-y} \\ f_{az-z} \end{bmatrix} = \begin{bmatrix} 0.005341 & -0.00006975 & -0.00006975 & 0 & 0 & 0 \\ -0.00006975 & 0.005341 & -0.00006975 & 0 & 0 & 0 \\ -0.00006975 & -0.00006975 & 0.005341 & 0 & 0 & 0 \\ 0 & 0 & 0 & 0 & -0.0001112 & 0.0001112 \\ 0 & 0 & 0 & 0.0001112 & 0 & -0.0001112 \\ 0 & 0 & 0 & -0.0001112 & 0.0001112 & 0 \end{bmatrix} \begin{bmatrix} f_{ax-x} \\ f_{ay-y} \\ f_{az-z} \\ f_{ax-x} \\ f_{ay-y} \\ f_{az-z} \end{bmatrix}. \quad (10a)$$

$$\begin{bmatrix} x_{ay} \\ y_{ay} \\ z_{ay} \\ \theta_{ay-x} \\ \theta_{ay-y} \\ \theta_{ay-z} \end{bmatrix} = \mathbf{C}_{a-a} \begin{bmatrix} f_{ax-x} \\ f_{ay-y} \\ f_{az-z} \\ f_{ax-x} \\ f_{ay-y} \\ f_{az-z} \end{bmatrix} = \begin{bmatrix} 1.280 \times 10^{-5} & 3.1193 \times 10^{-7} & -1.7446 \times 10^{-7} & 0 & 0 & 0 \\ -0.00006961 & 0.005367 & -0.00006961 & 0 & 0 & 0 \\ -1.7446 \times 10^{-7} & 3.1193 \times 10^{-7} & 1.280 \times 10^{-5} & 0 & 0 & 0 \\ 0 & 0 & 0 & 0 & -0.00008392 & 0.00008371 \\ 0 & 0 & 0 & 3.8288 \times 10^{-7} & 0 & -3.8288 \times 10^{-7} \\ 0 & 0 & 0 & -0.00008371 & 0.00008392 & 0 \end{bmatrix} \begin{bmatrix} f_{ax-x} \\ f_{ay-y} \\ f_{az-z} \\ f_{ax-x} \\ f_{ay-y} \\ f_{az-z} \end{bmatrix}. \quad (10b)$$

The above equations can clearly show the performance characteristics for any three-axis loading. For example, under a single force, the ratio of magnitude of the parasitic rotation about the X- (or Z-axis) to the primary translation along the Y-axis can be obtained based on Eq. (10a) as

$$\left| \frac{\mathbf{C}_{a-s}(4,5)}{\mathbf{C}_{a-s}(2,2)} \right| = \frac{0.0001112}{0.005341} = 2.08\%. \quad (11)$$

The cross-axis coupling effect, for example the effect of f_{ay-y} upon x_s , is then determined using Eq. (10a) by

$$\left| \frac{\mathbf{C}_{a-s}(1,2)}{\mathbf{C}_{a-s}(2,2)} \right| = \frac{0.00006975}{0.005341} = 1.31\%. \quad (12)$$

Moreover, the lost motion percentage under a single loading can be written using the results in Eqs. (10a) and (10b) as

$$\frac{\mathbf{C}_{a-a}(2,2) - \mathbf{C}_{a-s}(2,2)}{\mathbf{C}_{a-s}(2,2)} = \frac{0.005367 - 0.005341}{0.005341} = 0.49\%. \quad (13)$$

Equation (10a) shows that the force applied along an axis cannot produce the parasitic rotation about this axis. And two equal forces applied along two out of three axes, respectively, cannot cause the parasitic rotation about the third axis either.

In addition, simple comparisons, including kinetostatic and dynamic, between the analytical results and the FEA results (using Solidworks) are given in the Table 1, which shows good agreements in primary motion displacement, parasitic rotational angles, and modal frequency. There is relatively large difference only in cross-axis coupling motion, which may result from the error of the linear analytical modeling (or that of the FEA results), but have reasonable estimation in the changing trends.

4 Performance characteristics analysis

In this section, performance characteristics analysis for the monolithic decouple XYZ CPM as the motion stage (Fig. 2a) is conducted to see how the geometrical parameters' change can affect the performance characteristics and which performance characteristic is most sensitive to a geometrical parameter. This analysis will provide an initial optimization.

Figures 6, 7, and 8 illustrate the performance characteristics, defined in Eqs. (11), (12) and (13), against the normalized beam thickness, t , and the side-length, w , of the (cubic) stage under the conditions of specified material and beam length. Some key findings are summarized as follows.

- The parasitic rotation (Fig. 6) is influenced by both w and t , and increases with the increase of t and decreases with the increase of w . It is more sensitive to t compared with w . The smaller w is, the larger the effect of t on the parasitic rotation is. Similarly, the larger t is, the larger the effect of w on the parasitic rotation is.
- The cross-coupling (Fig. 7) is also affected by both w and t , and increases with the increase of t or with the decrease of w . It is also more sensitive to t in comparison with w . The smaller w is, the larger the effect of t on the cross-coupling is, and the larger t is, the larger the effect of w on the cross-coupling is.
- The lost motion (Fig. 8) is insensitive to w , and only is dominated by t . the smaller t , the smaller the lost motion is.

In addition, under the specified material, the translational motion range (same motion range along each axis) is only affected by the normalized beam thickness, t , and insensitive to the side-length, w , of the stage. The decrease of t can improve the motion range.

We can conclude from the above results that desired performance characteristics (large-range motion, minimized parasitic rotation, minimized cross-coupling and minimal lost motion) can be achieved by employing smaller t and appropriately larger w under the allowable conditions such as the minimum fabrication thickness, the overall system size, and stiffness/frequency requirements.

It is observed from Fig. 9 (or Eq. 9) that the first natural frequency goes up with the increase of t and/or the decrease of w , and is a little more sensitive to t . Therefore, in order to improve the natural frequency characteristic under small t and/or large w , we can enhance the system stiffness through using a better elasticity-average configuration with

Table 1. Comparisons of the analytical results and the FEA results.

Methods	Displacements under single loading: $F_y = 50\text{ N}$						Modal frequency (Hz)		
	X_s (mm)	Y_s (mm)	Z_s (mm)	θ_{sx} (rad)	θ_{sy} (rad)	θ_{sz} (rad)	First mode	Second mode	Third mode
Analytical results	-0.0049	0.3715	-0.0049	-3.87×10^{-4}	0	3.87×10^{-4}	284	284	284
FEA results	-0.0081	0.3884	-0.0077	-4.11×10^{-4}	-3×10^{-7}	4.20×10^{-4}	273	273	281
Difference (Analytical-FEA)/FEA	39.51 %	4.35 %	36.36 %	5.84 %	negligible	7.86 %	4.03 %	4.03 %	1.07 %

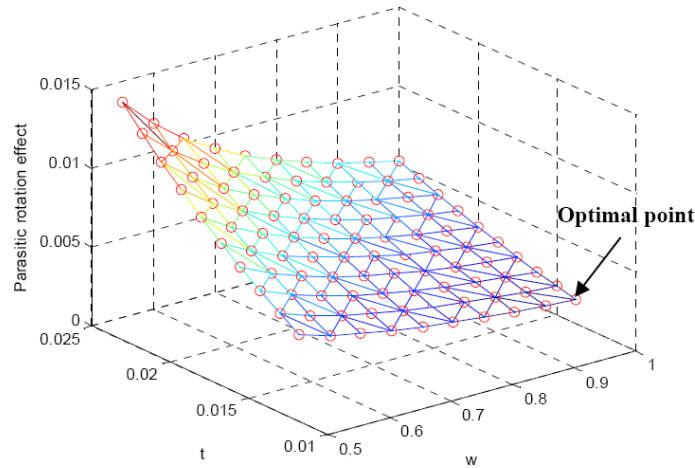


Figure 6. Parasitic rotation effect.

more beams in each spatial module as indicated in Fig. 2c, and/or reducing the mass of the cubic stages as indicated in Fig. 2b.

The motion of the variation (Fig. 5) in the coordinate system XYZ can be further determined by the following equations

$$\begin{aligned}
 Z &= (X_{1z}^2 + Y_{1z}^2 + Z_{1z}^2)^{0.5} \\
 \text{subject to } X_{1z} &= Y_{1z} = Z_{1z} \text{ with all positive values;} \\
 Y &= (X_{1y}^2 + Y_{1y}^2 + Z_{1y}^2)^{0.5} \\
 \text{subject to } Y_{1y} &= Z_{1y} \text{ with both negative values and} \\
 |Y_{1y}| &= 0.5X_{1y}; \\
 X &= (Y_{1x}^2 + Z_{1x}^2)^{0.5} \\
 \text{subject to } |Y_{1x}| &= |Z_{1x}| \\
 \text{with a positive } Z_{1x} \text{ and a negative } Y_{1x}
 \end{aligned} \tag{14}$$

where X, Y, and Z is the positive resultant motion in the coordinate system XYZ. X_{1z} , Y_{1z} , and Z_{1z} are the motion along the X_1 -, Y_1 -, and Z_1 -axes, respectively, in the coordinate system $X_1Y_1Z_1$ contributing to Z. Y_{1y} , and Z_{1y} are the motion along the Y_1 -, and Z_1 -axes, respectively, in the coordinate system $X_1Y_1Z_1$ contributing to Y. X_{1x} , Y_{1x} , and Z_{1x} are the motion along the X_1 -, Y_1 -, and Z_1 -axes, respectively, in the coordinate system $X_1Y_1Z_1$ contributing to X.

Let the motion range along each positive axis in the coordinate system $X_1Y_1Z_1$ be δ , the following constraint condi-

tions should be met:

$$\begin{aligned}
 0 &\leq X_1 = X_{1y} + X_{1z} \leq \delta; \\
 -\delta &\leq Y_1 = Y_{1x} + Y_{1y} + Y_{1z} \leq \delta; \\
 -\delta &\leq Z_1 = Z_{1x} + Z_{1y} + Z_{1z} \leq \delta.
 \end{aligned} \tag{15}$$

From the above results, it is directly obtained that the maximal single-axis motion along the positive X-axis is $2^{0.5}\delta$, the maximal single-axis motion along the positive Y-axis is $1.5^{0.5}\delta$, and the maximal single-axis motion along the positive Z-axis is $3^{0.5}\delta$.

The workspace for this variation in Octant I of the coordinate system XYZ can be obtained using numerical approach based on the above results (Eqs. 14 and 15), and is shown in Fig. 10. Note that the number of points in Fig. 10 depends on the set-up step size in the numerical approach.

5 Discussions

The large motion range requires a large-range linear actuator, which cannot be a PZT actuator. Although displacement amplifiers as actuated compliant P joints can be combined with the PZT actuators to enlarge the motion range, adversely, they lead to relatively low off-axis stiffness and augment the minimum incremental motion of the actuators, i.e. poor resolution. Thus, one needs to use the linear VC actuator for millimeter-level actuation range, which will generate heat to the mechanism.

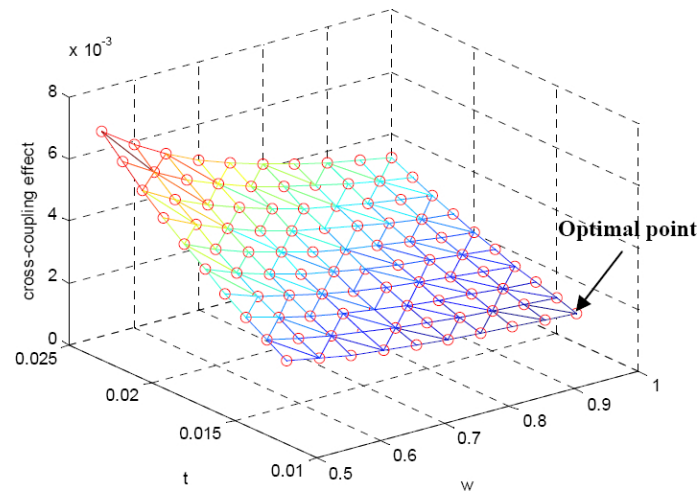


Figure 7. Cross-coupling effect.

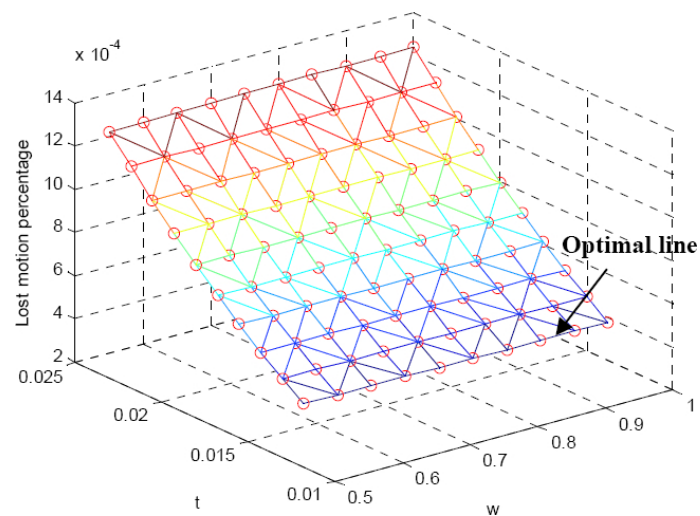


Figure 8. Lost motion percentage.

The monolithic design proposed in this paper is an over-constraint design in both the individual spatial multi-beam modules and the three identical legs. Although the problems of over-constraint are largely mitigated by the fact that the mechanism is monolithic and requires no assembly, there are still problems with its over-constraint. For instance, when VC actuators are used, the temperature will vary over the mechanism producing stress building up that can be problematic for precision performance. Moreover, when the mechanism heats up, the stage will drift as the design is not fully symmetric and thus not considered thermally stable.

6 Conclusions

This paper has presented and modelled a monolithic decoupled XYZ CPM (Fig. 2a) for multi-function applications: motion/positioning stages, acceleration/force sensors,

and energy harvesting devices. The proposed monolithic decoupled XYZ CPM uses only identical spatial multi-beam modules as the building blocks involving three geometrical parameters and can be fabricated by the planar manufacturing technologies (such as EDM) without assembly as the 2-D compliant mechanisms.

In addition, the monolithic decoupled XYZ CPM with improved natural frequency (Fig. 2b and c) and the variation with different motion range in each axis and same payload in each leg (Fig. 5) have been proposed. Redundant design for monolithic fabrication has been discussed in this paper, which can be used to extend the CPM's life.

The derived analytical kinetostatic models can capture the displacements of any stage under loading at any stage. The performance characteristics analysis for the motion stage application has been implemented to identify the optimal geometrical parameters for beam thickness and stage dimension.

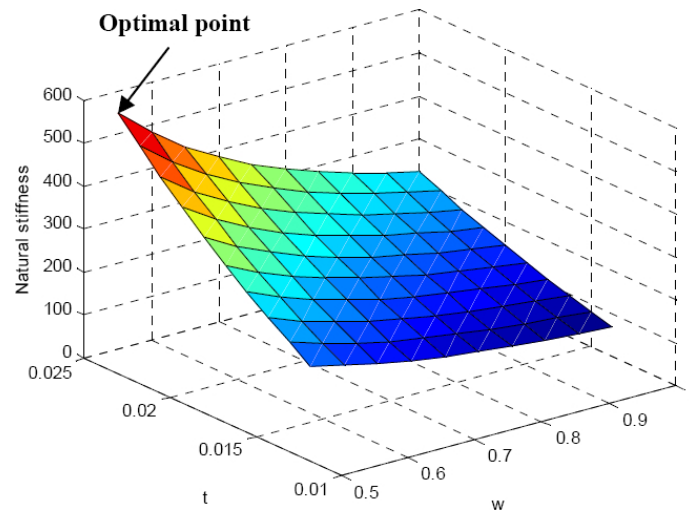


Figure 9. Natural frequency.

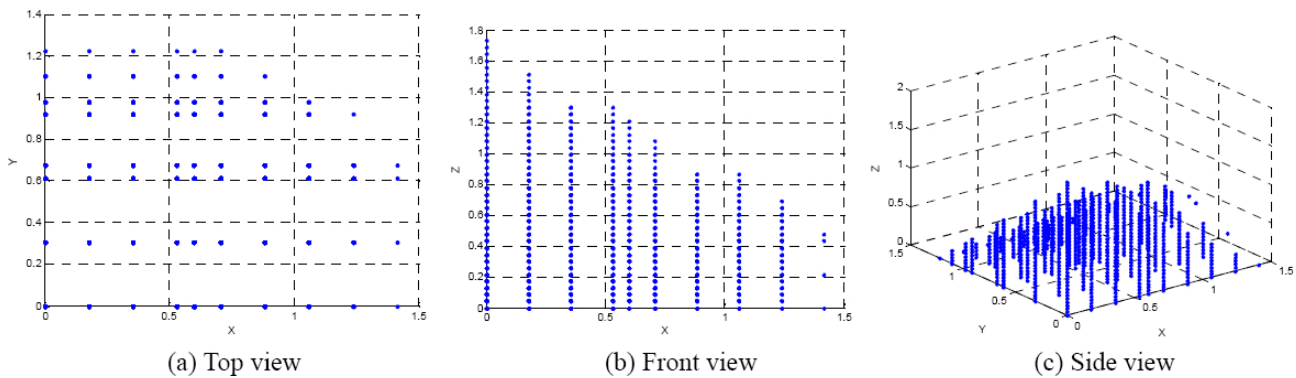


Figure 10. Workspace of the variation in Octant I of the coordinate system XYZ.

It is noted that the proposed design may promote the fabrication using the carbon nanotubes or carbon fibers, which may lead to novel compliant mechanisms used in the emerging MEMS or nano-electro-mechanical-systems (NEMS). Experiment verification, nonlinear modelling, fatigue analysis, and optimization deserve further investigation in the near future.

Acknowledgements. The author would like to sincerely appreciate the reviewers' valuable comments for improving the quality of this paper. Special thanks goes to Tim Power and Michael O'Shea for their excellent technical knowledge in fabricating the prototype in UCC.

Edited by: Y. Li

Reviewed by: H. Tang and one anonymous referee

References

- Ando, B., Baglio, S., Trigona, C., Dumas, N., Latorre, L., and Nouet, P.: Nonlinear mechanism in MEMS devices for energy harvesting applications, *J. Micromech. Microeng.*, 20, 125020, doi:10.1088/0960-1317/20/12/125020, 2010.
- Awtar, S.: Analysis and Synthesis of Planar Kinematic XY Mechanisms, Sc.D. thesis, Massachusetts Institute of Technology, Cambridge, MA, 2004.
- Awtar, S. and Slocum, A. H.: Constraint-Based Design of Parallel Kinematic XY Flexure Mechanisms, *J. Mech. Design*, 129, 816–830, 2007.
- Awtar, S., Ustick, J., and Sen, S.: An XYZ Parallel Kinematic Flexure Mechanism with Geometrically Decoupled Degrees of Freedom, *Journal of Mechanisms and Robotics*, 5, 015001, doi:10.1115/1.4007768, 2013.
- Cappelleri, D., Krishnan, G., Kim, C., Kumar, and V., Kota, S.: Toward the Design of a Decoupled, Two-Dimensional, Vision-Based uN Force Sensor, *Journal of Mechanisms and Robotics*, 2, 021010, doi:10.1115/1.4001093, 2010.
- Dong, W., Sun, L. N., and Du, Z. J.: Design of a Precision Compliant Parallel Positioner Driven by Dual Piezoelectric Actuators, *Sensor. Actuat. A-Phys.*, 135, 250–256, 2007.
- Gao, Z. and Zhang, D.: Design, Analysis and Fabrication of a Multidimensional Acceleration Sensor Based on Fully Decoupled Compliant Parallel Mechanism, *Sensor. Actuat. A-Phys.*, 163,

- 418–427, 2010.
- Hansen, B. J., Carron, C. J., Jensen, B. D., Hawkins, A. R., and Schultz, S. M.: Plastic Latching Accelerometer Based on Bistable Compliant Mechanisms, *Smart Mater. Struct.*, 16, 1967–1972, 2007.
- Hao, G.: Creative Design and Modelling of Large-Range Translational Compliant Parallel Manipulators, Ph.D. thesis, Heriot-Watt University, Edinburgh, UK, 2011.
- Hao, G. and Kong, X.: A 3-DOF Translational Compliant Parallel Manipulator Based on Flexure Motion, in: Proceedings of 2009 ASME International Design Engineering Technical Conferences & Computers and Information in Engineering Conference, San Diego, CA, USA, 30 August–2 September, DETC2009-86075, 2009.
- Hao, G. and Kong, X.: Novel XY Compliant Parallel Manipulators for Large Translation with Enhanced Out-of-Plane Stiffness, *J. Mech. Design*, 134, 061009, doi:10.1115/1.4006653, 2012a.
- Hao, G. and Kong, X.: Design and Modelling of a Large-Range Modular XYZ Compliant Parallel Manipulators Using Identical Spatial Modules, *Journal of Mechanisms and Robotics*, 4, 021009, doi:10.1115/1.4006188, 2012b.
- Hao, G. and Kong, X.: A Normalization-Based Approach to the Mobility Analysis of Spatial Compliant Multi-Beam Modules, *Mech. Mach. Theory*, 59, 1–19, 2013.
- Hao, G., Kong, X., and Reuben, R. L.: A Nonlinear Analysis of Spatial Compliant Parallel Modules: Multi-beam Modules, *Mech. Mach. Theory*, 46, 680–706, 2011.
- Howell, L. L.: *Compliant Mechanisms*, Wiley, New York, 2001.
- Kong, X. W. and Gosselin, C. M.: Kinematics and Singularity Analysis of a Novel Type of 3-CRR 3-DOF Translational Parallel Manipulator, *I. J. Robot. Res.*, 21, 791–798, 2002.
- Li, Y. and Xu, Q.: A Totally Decoupled Piezo-Driven XYZ Flexure Parallel Micropositioning Stage for Micro/Nanomanipulation, *IEEE T. Autom. Sci. Eng.*, 8, 265–279, 2011.
- Pham, H.-H., Yeh, H. C., and Chen, I.-M.: Micromanipulation System Design Based on Selective Actuation Mechanisms, *Int. J. Robot. Res.*, 25, 171–185, 2006.
- Rupp, C. J., Evgrafov, A., Maute K., and Dunn, M. L.: Design of Piezoelectric Energy Harvesting Systems: A Topology Optimization Approach Based on Multilayer Plates and Shells, *J. Intel. Mat. Syst. Str.*, 20, 1923–1939, 2009.
- Tang, X., Chen, I.-M., and Li, Q.: Design and Nonlinear Modeling of a Large-Displacement XYZ Flexure Parallel Mechanism with Decoupled Kinematics Structure, *Rev. Sci. Instrum.*, 77, 115101, doi:10.1063/1.2364132, 2006.
- Werner, C., Rosielle, P. C. J. N., and Steinbuch, M.: Design of a Long Stroke Translation Stage for AFM, *International Journal Machine Tools and Manufacture*, 50, 183–190, 2010.
- Yue, Y., Gao, F., Zhao, X., and Ge, Q.: Relationship among Input-Force, Payload, Stiffness and Displacement of a 3-DOF Perpendicular Parallel Micro-Manipulator, *Mech. Mach. Theory*, 45, 756–771, 2010.